Available online at www.eccomasproceedia.org
Eccomas Proceedia SMART (2023) 128-139

ECCOMAS
Proceedia

X ECCOMAS Thematic Conference on Smart Structures and Materials
SMART 2023
D.A. Saravanos, A. Benjeddou, N. Chrysochoidis and T. Theodosiou (Eds)

# SHUNTED PIEZOELECTRIC PATCH ADAPTIVE VIBRATION ABSORBER SET TO MAXIMISE ELECTRIC POWER ABSORPTION

**P. GARDONIO*, G. K. RODRIGUES**

Università degli Studi di Udine - DPIA
Via delle Scienze 206, 33100, Udine, Italy
* e-mail: paolo.gardonio@ uniud.it

**Abstract**. This paper presents a comprehensive study on a shunted piezoelectric patch adaptive vibration absorber, which can be bonded in batches on thin-walled structures to control the broad-band resonant response of low order flexural modes. The self-contained control unit is formed by a thin piezoelectric patch connected to a shunt encompassing a parallel RL network. The inductive and resistive components of the shunt are adapted online in such a way as to maximise the time-averaged electric power absorbed by the shunt. The paper shows that this tuning cost function corresponds to minimising the time-averaged total flexural response of the hosting structure. Moreover, it shows that the cost function is characterised by a bell-shape with principal directions along constant-inductance and constant-resistance values. Hence, it is proposed a two paths online tuning strategy where the inductance is tuned first along a constant-resistance path and then the resistance is tuned along the resulting constant-inductance path with an extremum seeking gradient search algorithm. The paper presents experimental results for a test rig composed by a rectangular flat plate equipped with five piezoelectric patches connected to the self-tuning shunts. On-line experiments have shown that the proposed local tuning of the five piezoelectric patches generates reductions of the resonant responses of the first, second and fourth flexural modes of the order of 14 dB, 4 dB, 8 dB.

**Key words**: Semi-active vibration control; Piezoelectric vibration absorber; Shunted piezoelectric patch; Self-tuning shunt; Online tuning shunt; Extremum seeking algorithm.

## 1 INTRODUCTION

This paper is focused on the control of the flexural vibration and sound radiation by thin structures with self-contained units formed by a piezoelectric patch transducer connected to a resistive-inductive shunt circuit [1-5]. The goal of the study is to devise self-contained, compact, and lightweight vibration control units, which can be bonded in batches on thin-walled lightweight structures. Each unit can then be set to control the resonant response of a distinct low-order flexural mode. In this way, both the flexural vibration and the sound radiation of the structure can be effectively reduced at low audio frequencies where, due to the low modal overlap [6], the overall response is indeed characterised by the resonant responses of the target low-order flexural modes.


Peer-review under responsibility of the organizing committee of SMART 2023.
doi: 10.7712/150123.9771.444237

The resistive-inductive effects of the shunt combined with the capacitive effect of the piezoelectric element generate via the piezoelectric transduction a combined inertia-stiffness-damping action on the hosting mechanical system, which can be used to produce a piezoelectric vibration absorption effect [1-5]. With this arrangement self-tuning algorithms can be implemented, which vary online the resistive and inductive components of the shunt in such a way as the fundamental natural frequency and damping ratio of the resulting shunted piezoelectric vibration absorber are continuously adapted to changes of the dynamic response of the hosting structure [7-9]. This paper builds up on Refs. [10-12] and presents an experimental study on the control of the resonant response of a target low-order flexural mode of a thin panel structure equipped with five self-tuning vibration absorbers formed by a piezoelectric patch connected to a tuneable shunt composed by a resistor and inductor connected in parallel (RL-shunt). The shunt is set to maximise the electric power absorption, that is the electric power dissipation in the resistor, from the resonant response of the target flexural mode. This tuning law was successfully investigated for control units formed by a coil-magnet transducer connected to a RL shunt [10]. The two-paths online tuning approach proposed in Ref. [11,12] is employed here, where the inductance and resistance of the shunts are tuned sequentially with an extremum seeking gradient search algorithm [13] in such a way as to maximise the time-averaged electric power absorption from the resonant response of the target low-order flexural mode of the panel.

## 2 PLATE STRUCTURE WITH THE FIVE CONTROL UNITS

Figure 1 shows the thin flat rectangular panel hosting structure, which is made of steel. Five thin square MFC piezoelectric patches are bonded on the panel with the terminals connected via ad hoc interface circuits to a multi-channel dSPACE digital board used for the online implementation of the five self-tuning RL-shunts. The panel is fixed to a rigid frame and is excited by a transverse point force exerted by a shaker via a stinger equipped with a force cell. The geometry and physical properties of the panel and five piezoelectric patches are summarised in Table 1. It should be emphasised that this is a laboratory apparatus for research purposes. In practice, the self-tuning shunts should be developed into miniaturised analogue circuit boards, which could be embedded on the piezoelectric patches.

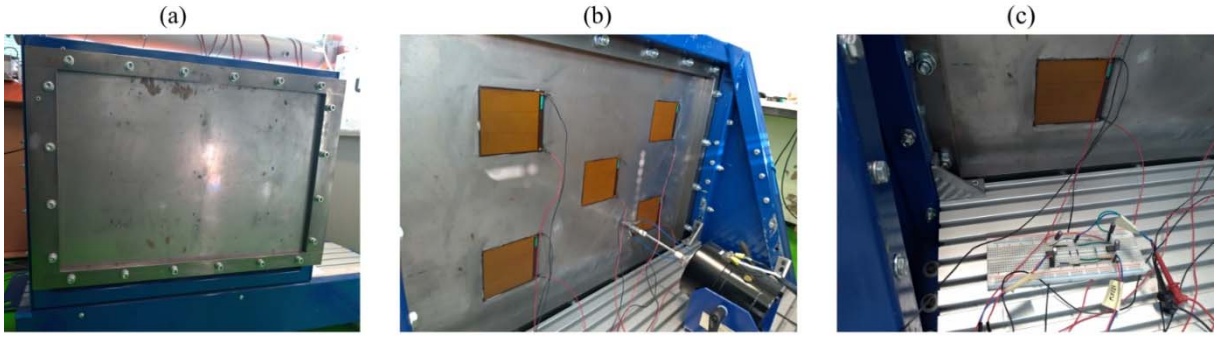


**Figure 1**: Thin panel model structure (a), which is equipped with five piezoelectric patches (b) connected to a digital shunt via an interface circuit (c)

**Table 1**: Dimensions and physical properties of the panel and piezoelectric patches.

| Parameter | Plate | Piezoelectric patches |
|---|---|---|
| dimensions | $l_{xp} \times l_{yp} = 668 \times 443\ mm$ | $l_{xpe} \times l_{ype} = 85 \times 85\ mm$ |
| thickness | $h_p = 1.8\ mm$ | $h_{pe} = 0.3\ mm$ |
| material | $steel$ | $MFC$ |
| point force position | $x_p = 0.63\ l_{xp}\ ,\ y_p = 0.25 l_{yp}$ | |
| patches centre position | | $x_{pe1} = l_{xp}/2\ ,\ y_{pe1} = l_{yp}/2$<br>$x_{pe2,3,4,5} = l_{xp}/2 \pm \Delta_x\ ,\ y_{pe2,3,4,5} = l_{yp}/2 \pm \Delta_y$<br>$\Delta_x = 185\ mm\ ,\ \Delta_y = 117.5\ mm$ |

## 2.1 Tuneable digital shunts

As shown in Figure 2a,b, the five piezoelectric patches are connected to self-tuning shunts composed by a resistor and inductor connected in parallel. Each shunt is tuned locally to maximise the time-averaged electric power absorbed by the shunt itself, which, as shown in Figure 2b, is derived from the voltage drop across the resistor of the shunt [11,12]. Each shunt is set to maximise the electric power absorption from the resonant response of a target low-order flexural mode of the plate. To this end, the electric power is filtered with a band-pass filter centered at the resonance frequency of the target mode. The bandwidth of the filter is selected in such a way as it incorporates the resonant response of the target mode only. It is important to recall here, that the proposed control unit is meant to work at low audio frequencies, where the flexural response of the panel is characterised by a low modal density such that there is no frequency overlap between the resonant responses of neighbor flexural modes of the structure [6]. Therefore, recalling that the hosting structure is lightly damped, the filters were selected in such a way as to have about a 20 dB bandwidth with respect to the resonance peak of the target mode.

The five self-tuning shunts are implemented online in a multi-channel digital board, which, as shown in Figure 2c, is connected to the five piezoelectric patches through five interface circuits [14]. More specifically, as shown in Figure 2c, the terminals of each piezoelectric patch

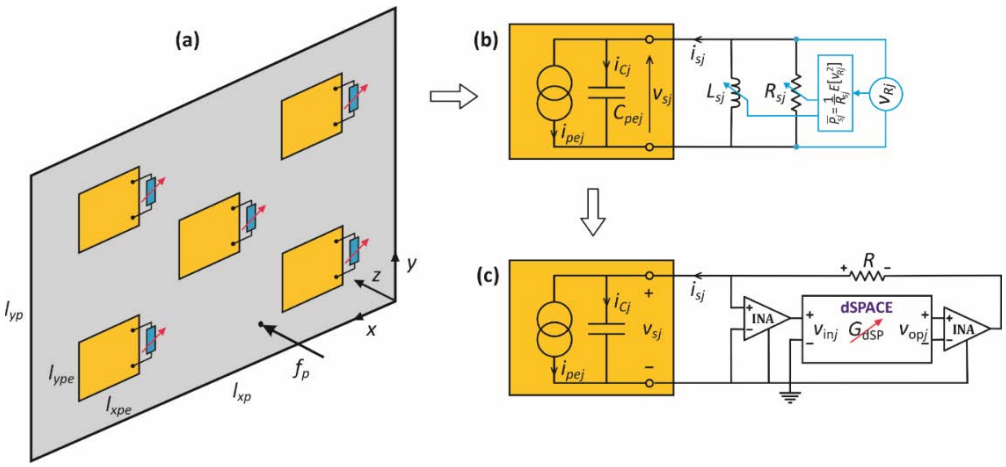


**Figure 2**: Panel with five piezoelectric patches (a) connected to RL self-tuning shunts (b) implemented in a dSPACE digital board (c).

are connected to the input channels of the digital board via a high input impedance instrumentation amplifier, which feeds to the board the shunt voltage without influencing the current flow through the terminals. Each output channel of the digital board is then connected to the terminals of the respective piezoelectric patch via a high input impedance instrumentation amplifier, which ensures the output voltage from the board is turned by the resistor $R_{oj}$ into a given shunt current flow through the terminals of the piezoelectric patch. In this way, the desired shunt impedance can be generated on each piezoelectric patch by suitably synthesising the transfer function $G_{sj}(s)$ between the input and output channel pairs of the digital board (here $s$ is the Laplace variable). As shown in Refs. [12,14] the interface circuit and dSPACE assembly generates the following electrical impedance effect (here $\omega$ is the circular frequency):

$$Z_{sj}(\omega) = \frac{v_{sj}(\omega)}{i_{sj(\omega)}} = \frac{R_{oj}}{1-G_{sj}(\omega)}, \tag{1}$$

where $v_{sj}(\omega)$, $i_{sj}(\omega)$ are the complex amplitudes of the shunt voltage and current and of the digital board input and output voltages. Also, $G_{sj}(\omega)$ is the frequency response function (FRF) implemented in the digital board. This equation can be reworked to give the FRF $G_{sj}(\omega)$ that should be implemented in the digital board to generate the desired shunt electrical impedance effect:

$$G_{sj}(\omega) = \frac{v_{\mathrm{op}j(\omega)}}{v_{\mathrm{in}j(\omega)}} = 1 - \frac{R_{oj}}{Z_{sj}(\omega)}. \tag{2}$$

Hence, to generate the desired parallel RL shunt impedance effect with resistance $R_{sj}$ and inductance $L_{sj}$, such that the electrical impedance FRF is given by

$$\frac{1}{Z_{sj}(\omega)} = \frac{1}{R_{sj}} + \frac{1}{j\omega L_{sj}}, \tag{3}$$

the following FRF should be synthesized in the digital board

$$G_{sj}(\omega) = 1 - \frac{R_{oj}}{R_{sj}} - \frac{R_{oj}}{j\omega L_{sj}} = \frac{j\omega(R_{sj}-R_{oj})L_{sj}-R_{oj}R_{sj}}{j\omega R_{sj}L_{sj}}. \tag{4}$$

In practice, the dSPACE board was operated through a Real-Time-Interface, which implemented a MATLAB–Simulink model of the desired transfer functions $G_{sj}(s)$ between the dSPACE input and output ports connected to the piezoelectric patches. To minimise high frequency noise effects and to ensure the transfer function implemented digitally is guaranteed to be proper, the transfer function $G_{sj}$ was modified in such a way as it encompasses a low-pass filtering effect with the corner frequency set at 500 Hz. This value was chosen in such a way as the digital shunt can work in the 20 – 140 Hz frequency range where the flexural response of the panel is characterised by a low modal density and thus the resonant response of the target flexural mode does not overlap with those of neighbor modes [6]. Overall, the transfer functions implemented in the dSPACE board were given by the following FRF

$$G_{sj}(\omega) = \frac{j\omega\left(R_s-R_{oj}\right)L_s\omega_{lp,s}-R_{oj}R_s\omega_{lp,s}}{\left(j\omega\omega_{lp,s}-\omega^2\right)R_sL_s}, \tag{5}$$

where $\omega_{lp,s}$ is the corner frequency of the low-pass filter.

## 2.2 Cost functions

The shunted piezoelectric units are set to control the time-averaged resonant response of a target flexural mode when the hosting plate structure is exposed to a stationary stochastic excitation. Therefore, two cost functions were considered in this study. First, the so-called "reference cost function" given by the time-averaged and spatially-averaged flexural vibration of the structure,

$$\bar{K}(R_{sj}, L_{sj}) = E\big[K(R_{sj}, L_{sj}, t)\big], \tag{6}$$

which has been used to monitor the response of the panel. Here, $E[\ \ ]$ is the expectation operator and $K(R_{sj}, L_{sj}, t)$ is the instantaneous flexural kinetic energy of the panel, which has been estimated from transverse velocities $\dot{w}_i$ measured with a laser vibrometer at a grid of $N$ points

$$K(t) = \frac{1}{2N} M_p \sum_{i=1}^{N} \dot{w}_i^2(t)\ , \tag{7}$$

where $M_p$ is the mass of the plate. Second, the so-called "tuning cost function" given by the time-averaged vibration energy absorbed by each shunted piezoelectric patch

$$\bar{P}(R_{sj}, L_{sj}, t) = E\big[P(R_{sj}, L_{sj}, t)\big], \tag{8}$$

which has been used to tune the resistive and inductive components of the shunt. Here $P(R_{sj}, L_{sj}, t)$ is the instantaneous electric power absorbed by the shunt, that is the electric power dissipated by the shunt resistor, which, therefore, has been derived from the voltage drop across the shunt, $v_{Rj}$, and the resistance in the shunt $R_{sj}$

$$P\big(R_{sj}, L_{sj}, t\big) = \frac{1}{R_{sj}} v_{Rj}^2(t). \tag{9}$$

The two functions $\bar{K}(R_{sj}, L_{sj})$ and $\bar{P}(R_{sj}, L_{sj}, t)$ were derived from measurements of the panel velocities and of the shunt voltages duly filtered with a band-pass filter centered at the resonance frequency of the target mode.

## 3 TUNING ANALYSIS – GLOBAL VERSUS LOCAL

To start with, this section presents a tuning analysis for the case where all piezoelectric patches are connected to individual RL-shunts set to control the resonant response respectively of the first, second and fourth flexural modes of the panel (the third mode is weakly excited by the shaker point force). To this end, RL-maps have been built from a vast measurement campaign for the reference and tuning cost functions, that is the time-averaged total flexural kinetic energy $\bar{K}_r(R_{sj}, L_{sj})$ and the the time-averaged electric power absorbed by the shunt $\bar{P}_r(R_{sj}, L_{sj})$, band filtered at the resonance frequency of the $r$-th mode. Here the objective is to verify if the minimum of $\bar{K}_r(R_{sj}, L_{sj})$ and the maximum of $\bar{P}_r\big(R_{sj}, L_{sj}\big)$ occur for the same values of the shunt resistance $R_{sj}$ and inductance $L_{sj}$.

Figure 3 shows the measured maps of the reference cost function $\bar{K}_r(R_{sj}, L_{sj})$ and tuning cost function $\bar{P}_r(R_{sj}, L_{sj})$ when the shunts are set to control the resonant response of the first, second and fourth flexural modes (i.e. $r = 1,2,4$). For all three modes, the map of $\bar{K}_r$ is characterised by a non-convex inverse bell-shape with a single minimum whereas the map of $\bar{P}_r$ has a mirror non-convex bell-shape with a single maximum. As highlighted by the cross and circular markers, the points of minimum of $\bar{K}_r$ and maximum of $\bar{P}_r$ closely overlap in the maps. The

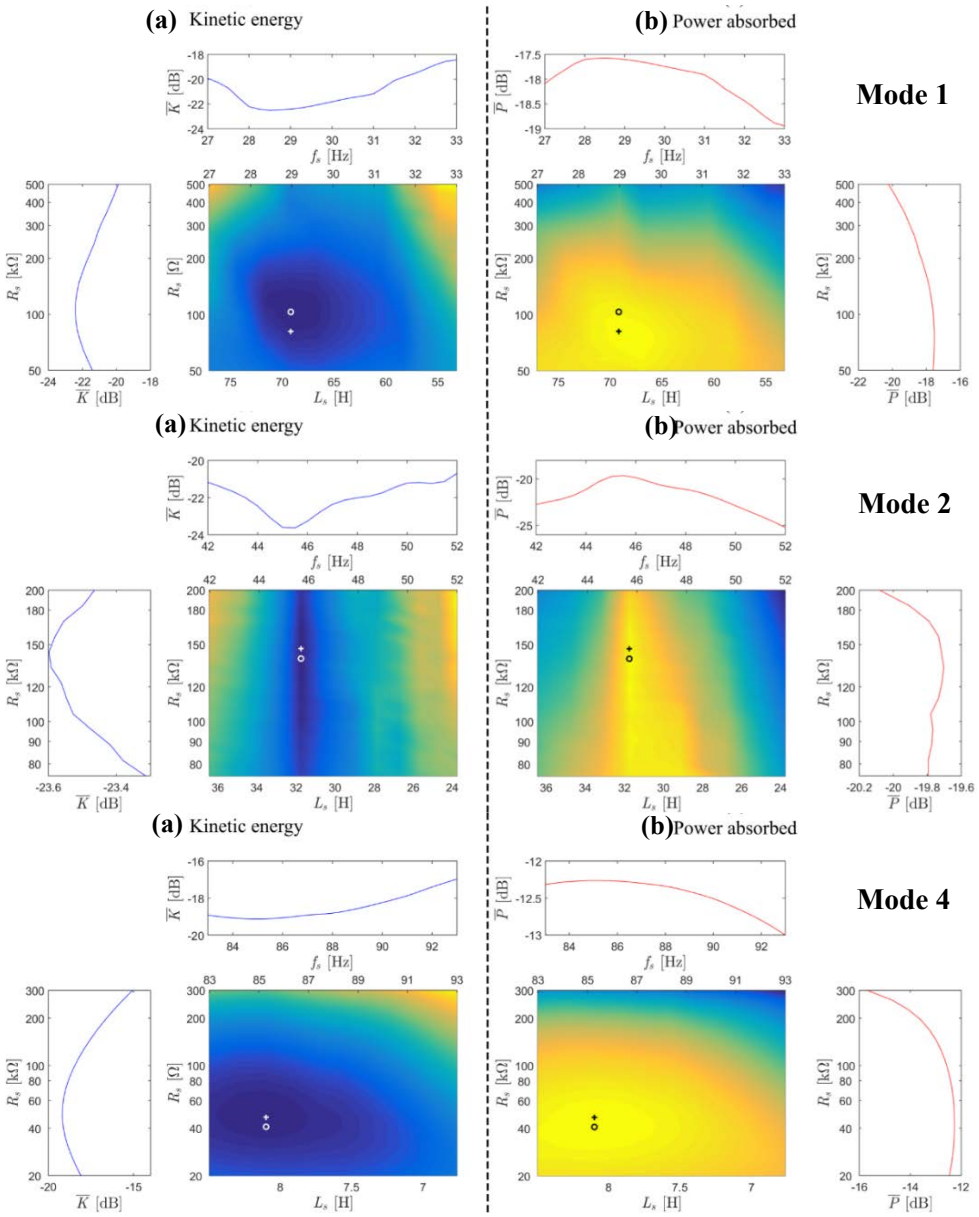


**Figure 3:** Measured maps of $\overline{K}(R_s, L_s)$ (a) and $\overline{P}(R_s, L_s)$ (b) when the shunts are set to control the resonant response of mode 1 (top), mode 2 (centre), mode 4 (bottom), with slice cuts at optimal constant resistance and constant inductance.

roughness on the maps is due to the lengthy measurement procedure necessary to produce the maps [12]. Nevertheless, the maps clearly indicate that the minimum of $\overline{K}_r$ and the maximum of $\overline{P}_r$ are rather close to each other. Besides, the two maps are quite flat in the vicinity of minimum/maximum points and thus the non-perfect alignment of the minimum of $\overline{K}_r$ and the maximum of $\overline{P}_r$ can be considered negligible. In conclusion, the measurement results show that, considering the resonant response of well-separated low-order flexural modes of the structure

[6], the minimum of the plate time-averaged total flexural kinetic energy and the maximum of the time-averaged electric power absorbed by the shunt are characterised by close values of the optimal shunt resistance and close values of the optimal shunt inductance. Hence, as found with simulations in Refs. [11,12], to minimise the time-averaged total flexural kinetic energy, that is the time-averaged and spatially-averaged flexural response of the structure, the resistance and inductance of the shunt should be tuned to maximise the time-average electric power absorbed by the shunt itself. The RL-shunt can thus be tuned locally without the need of measuring the flexural response of the target mode of the structure. It is sufficient to measure the electric power absorbed by the shunt, which, as depicted in Figure 2b and given in Eq. (9), can be suitably estimated from the voltage drop across the shunt resistor.

A thorough analysis of the kinetic energy and power cost functions shows that the two maps are characterised by constant resistance and constant inductance principal directions [11,12]. Hence, the tuning can be carried out in two steps where, starting from arbitrary initial values of the shunt resistance and inductance $(R_{sj,ini}, L_{sj,ini})$, the optimal inductance $L_{sj,opt}$ is first searched along the path $R_{sj} = R_{sj,ini}$ and then the optimal resistance is searched along the path $L_{sj} = L_{sj,opt}$. This two-paths tuning strategy can be implemented online such that convergence to the optimal RL values would be guaranteed, too, in presence of variations of the dynamic response of the structure and changes of the shunt response. The lateral and top graphs beside the two maps show that the constant resistance $R_{sj} = R_{sj,opt}$ and constant inductance $L_{sj} = L_{sj,opt}$ paths on the kinetic energy cost function are characterised by inverse bell shapes whereas the same paths on the power cost function are characterised by bell shapes. The tuning of the shunt components will thus involve a search of the maximum along non-convex bell-shaped paths, which, can be suitably implemented with an extremum seeking algorithm [13].

## 4. ONLINE IMPLEMENTATION OF THE SELF-TUNING SHUNTS

The online implementation of the two-paths self-tuning approach to maximise the electric power absorption by each shunt is now investigated considering the smart panel setup described in Section 2, and depicted in Figure 1, is excited with a stationary white noise stochastic primary force excitation. The shunts are tuned to control in turn the resonant response of the first, second and fourth flexural modes of the plate with the power function filtered between $\omega_{nr} - \Delta\omega_r/2$ and $\omega_{nr} + \Delta\omega_r/2$, where the centre frequencies and bandwidths are given in Table 2.

The tuning is implemented in parallel, i.e. all the shunts are tuned simultaneously. More specifically, for each unit the two-paths tuning strategy discussed above is implemented starting from the initial values of the shunt components $R_{sj,ini}, L_{sj,ini}$ reported in Table 2. The optimal inductance $L_{sj,opt}$ is first searched along the path $R_{sj} = R_{sj,ini}$ starting from $R_{sj,ini}, L_{sj,ini}$. Then, the optimal resistance $R_{sj,opt}$ is sought along the path $L_{sj} = L_{sj,opt}$ starting from $R_{sj,ini}, L_{sj,opt}$. The searches along the two paths are implemented using the extremum seeking algorithm [13]. This is a model-free gradient driven search algorithm, which asymptotically leads to the maximum of the non-convex bell-shaped paths with $R_{sj} = \text{const}$ and $L_{sj} = \text{const}$. Since the tuning process is asymptotic, the search along each path was stopped as the increment of the absorbed power fell below the threshold $\varepsilon_P$ reported in Table 2.

**Table 2**: Experimental data for the online tuning procedure

| Parameter | Value | Parameter | Value |
|---|---|---|---|
| 1st mode resonant frequency | $\omega_{n1} = 29.8\ Hz$ | Band-pass frequency width | $2\Delta\omega_r = 20\ Hz$ |
| 2nd mode resonant frequency | $\omega_{n2} = 45.9\ Hz$ | Power threshold value | $\varepsilon_P = 0.05$ |
| 4th mode resonant frequency | $\omega_{n4} = 88.4\ Hz$ | Dither frequency | $\omega_d = 0.7\ Hz$ |
| Initial guess, 1st mode tuning | $R_{s,ini} = 400k\Omega, L_{s,ini} = 72H$ | High-pass filter frequency | $\omega_{hp} = 0.03\ Hz$ |
| Initial guess, 2nd mode tuning | $R_{s,ini} = 100k\Omega, L_{s,ini} = 25H$ | Low-pass filter frequency | $\omega_{lp} = 0.02\ Hz$ |
| Initial guess, 4th mode tuning | $R_{s,ini} = 70k\Omega, L_{s,ini} = 6H$ | | |

## 4.1 Extremum seeking tuning algorithm

The sketch in Figure 4 exemplifies the two-paths tuning search implemented in each shunt with the extremum seeking algorithm [13]. The tuning of the shunt inductance (L-tuning) and resistance (R-tuning) are implemented sequentially with the same procedure. Therefore, for simplicity, the algorithm is described with reference to the L-tuning only. As discussed above, both the shunt and the extremum seeking algorithm are implemented digitally in the multi-channel dSPACE board. Therefore, the whole scheme in Figure 4 assumes the parameters are discretised. As sketched in the figure, the electric power absorbed by the shunt, $P_{sj,\mathrm{i}}$, is derived from the voltage drop across the shunt resistor, that is the shunt voltage $v_{sj,\mathrm{i}}$. The power signal is then averaged over the past $N_s$ samples and sent to the extremum seeking loop to generate the inductance tuning parameter. This algorithm belongs to the perturb-and-observe type algorithms. Hence, the tuning parameter $L_{sj,\mathrm{i}}$ is modulated with a low frequency harmonic signal $z_{d,\mathrm{i}} = Z_0 sin(\omega_d t_i)$. As a result, the electro-mechanical response of the plate and shunted piezoelectric patch, and thus the electric power absorbed by the shunt, show the time-harmonic dithering effect. More precisely, when the tuning parameter is lower than the optimal value, i.e., $L_{sj,\mathrm{i}} < L_{sj,opt}$, the wavy power signal is in-phase with the dithering signal. Conversely, when the tuning parameter is higher than the optimal value, i.e., $L_{sj,\mathrm{i}} > L_{sj,opt}$, the wavy power

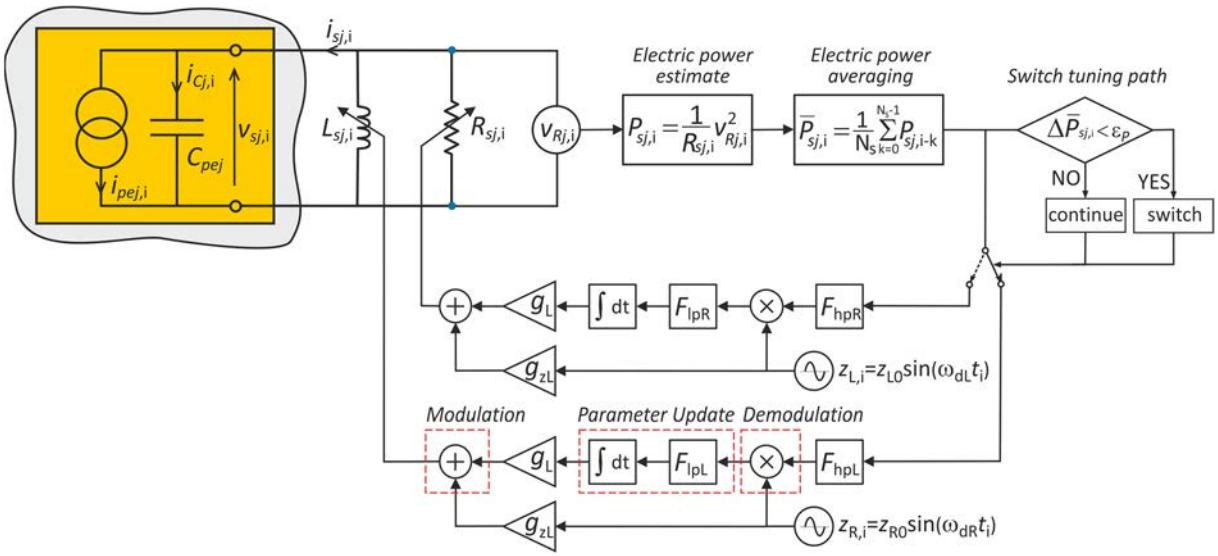


**Figure 4:** Block diagram of the two-paths extremum seeking gradient search algorithm.

signal is out-of-phase with the dithering signal. The wavy power signal can thus be used to update the inductance parameter. To this end, the signal is first passed through a high-pass filter $F_{hpL} = \frac{j\omega}{j\omega+\omega_{hp}}$ to remove the bias ($\omega_{hp}$ is the filter corner frequency). The resulting signal is then demodulated by multiplying it with the same dithering signal $z_{L,\mathrm{i}}$ used in the modulation phase. The resulting wavy signal will be either mostly positive for $L_{sj,\mathrm{i}} < L_{sj,opt}$ or mostly negative for $L_{sj,\mathrm{i}} > L_{sj,opt}$. The updated tuning parameter $L_{sj,\mathrm{i}}$ is then generated by integrating this signal after it has been passed through a low pass filter $F_{lpL} = \frac{1}{j\omega+\omega_{lp}}$ to remove the effects of noise and higher frequency harmonics. The increment or decrement of the updated tuning parameter will be proportional to the slope of the cost function such that fast convergence will be guaranteed along the side branches of the bell-shaped cost function and slow, but precise, tuning will be ensured close to the peak of the cost function where the bell-shape is flatter. This algorithm is bound to converge and oscillate around the maximum value of the power cost function. Therefore, to stop the search along one path and move forward to the search along the other path, as shown in the sketch of Figure 4, a switching loop is added to the algorithm such that, when the increment of the averaged absorbed power $\Delta\bar{P}_{sj,i} = \frac{|\bar{P}_{sj,i}-\bar{P}_{sj,i-1}|}{\bar{P}_{sj,i-1}}$ is below a given threshold $\varepsilon_P$, the search is switched to the other path. It is important to highlight here that the time-window for the $N_s-\mathrm{samples}$ time-averaging of the absorbed electrical power is much shorter than the period of the dithering signal for the extremum seeking tuning. Thus, it does not interfere with the dithering tuning signal of the extremum seeking algorithm.

### 4.2 Online tuning

The on-line implementation of the extremum seeking algorithms set to maximise in each control unit the electrical power absorbed by the shunt is finally discussed in this subsection for the cases where the shunts are tuned to control in turn the resonant responses of the first, second and fourth flexural modes of the plate. Figure 5 shows evolutions in time of the resistance and inductance of the shunt connected to the centre patch set to maximise the time-averaged electric power absorbed from the resonant response of the first, second and fourth resonant flexural modes. The three plots show that the tuning of the resistance is much faster than the tuning of the inductance. In this respect, it should be highlighted that a very fine tuning was searched here, that is a fairly small threshold $\varepsilon_P$ was considered. As can be noticed in the maps of Figure 3, the monitor and control cost functions are characterised by rather flat surfaces close to the optimal tuning points. Therefore, it is expected that, even with larger threshold $\varepsilon_P$, the tuning algorithm will converge to shunt resistance and inductance values that generate nearly optimal electric power absorption and thus nearly optimal reductions of the resonant responses of the target modes. It is important to emphasize here that the online tuning is implemented for the case where the panel is exposed to a stochastic broadband excitation. Therefore, to have a proper estimate of the time-averaged electric power absorbed by the shunt, rather long time-averages should be implemented. In this respect, to avoid too long convergence times, the length of the time averages was taken equal to $\mathrm{ns} = 12$ samples, that is $0.8$ s. With this choice, convergence to the optimal tuning parameters was reached in a reasonable timescale, although

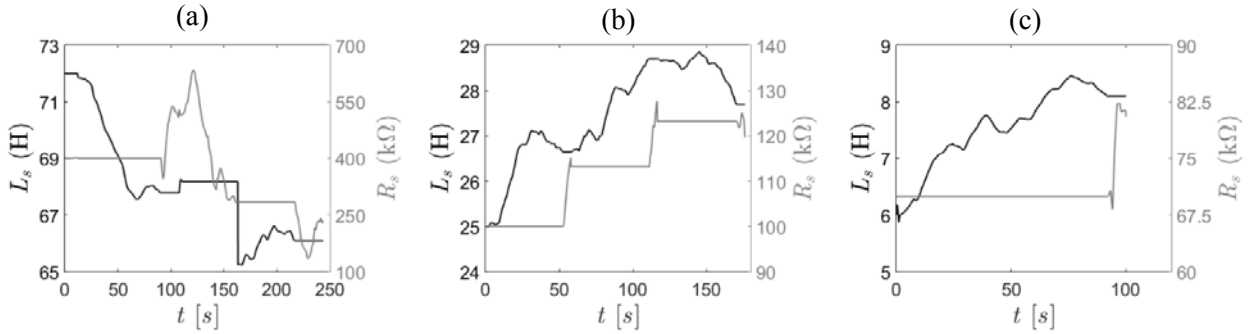


**Figure 5:** Evolutions of the resistance and inductance of the shunt connected to the centre patch when the extremum seeking algorithm is implemented to maximise the time-averaged electric power absorption from the resonant response of the first (a), second (b) and fourth (c) flexural modes.

at the cost of losing some accuracy when the random excitation undergoes rapid and substantial changes. The three graphs show that the tuning time for each mode is different. This is due to two factors. First, the distance from the optimal values of the initial guess for the shunt resistance and inductance was different for the three modes. Second, the profile of the bell shaped cost function was different for the three modes. As a result, a different number of iterations was required before the algorithm climbed to the top of the bell-shaped cost functions to find the optimal inductance and resistance values.

The control effects produced by the shunted piezoelectric patches are now investigated with reference to two configurations where the shunts either implement very large resistances to mimic open circuits or implement the optimal resistances and inductances found with the extremum seeking tuning algorithm set to maximise the electric power absorption from the resonant responses of the first, second and fourth flexural modes respectively. The left hand side column in Figure 6 shows the total flexural kinetic energy derived from measurements of the transverse velocities taken at a grid of $4 \times 4$ points with a scanner laser vibrometer. The right hand side column in Figures 6 shows, for the centre control unit, the electric power absorbed by the shunt estimated from the voltage drop across the terminals of the shunt and the resistance implemented in the shunt. To better emphasise the vibration control effects produced by the shunted piezoelectric patches, the force excitation and the measured responses of the panel and shunt were filtered with a 20 Hz band pass filter centered at the target resonance frequency. Also, to allow a fair comparison, the same stochastic force excitation was implemented to produce the results with open circuit and shunted piezoelectric patches.

The left hand side plots in Figure 6 show that the amplitude of the panel total flexural kinetic energy (i.e. its spatially averaged flexural vibration) is substantially reduced when the units are set to control the resonant response of the first and fourth flexural modes of the panel (top and bottom graphs). Considering time-average levels taken over the $13\ s$ time- acquistion, the ratios of the kinetic energy when the units are optimally shunted and in open circuit are of the order of $\overline{K}_{sh}/\overline{K}_{oc} = 0.2$ for mode 1, $\overline{K}_{sh}/\overline{K}_{oc} = 0.63$ for mode 2 and $\overline{K}_{sh}/\overline{K}_{oc} = 0.4$ for mode 4, which, translated into dB, result in reductions of 14 dB, 4 dB, 8 dB respectively. These results are in line with the reductions found with the spectral analysis presented in Ref. [12] and thus confirm both the validity of the proposed tuning approach based on the maximisation of the electric power absorption of the shunt and the effectiveness of the extremum seeking tuning algorithm.

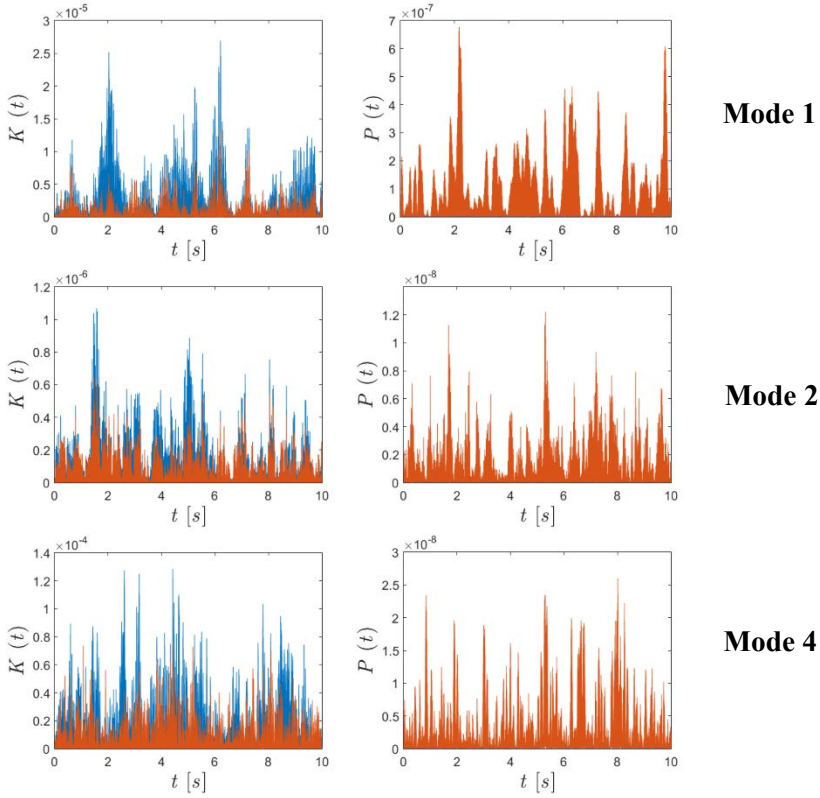


**Figure 6:** Measures of the panel flexural kinetic energy (left hand side) and electric power absorbed by the shunt (right hand side) connected to the centre patch when the plate is excited by a stochastic excitation and the patches are either in open circuit (blue lines) or connected to shunts (red lines) set to maximise the time-averaged electric power absorption from the resonant response of the first (top graphs), second (centre graphs) and fourth (bottom graphs) flexural modes.

The right hand side graphs in Figure 6 show that the absorbed power rises significantly when the shunt is indeed set to maximise the time-averaged electric power absorption. In fact, the graphs seem to show only the electric power absorbed when the shunts are optimally tuned (orange line). As a matter of fact, the graphs report the electric power absorbed when the shunts are in open circuit too, although the values are so small compared to those of the power absorbed by the optimally tuned shunt that the lines are merely visible (blue lines).

## 5. CONCLUSIONS

This paper has investigated the implementation on a flat rectangular panel of a self-contained vibration control unit formed by a piezoelectric patch connected to a RL self-tuning shunt, which can be bonded on thin structures to control the resonant response of a distinctive target flexural mode due to broadband excitations. The study has proven that the shunts can be conveniently tuned locally by maximising the electric power absorbed by the shunts from the resonant response of the target flexural mode to be minimised. A two-step tuning approach has thus been proposed, where the extremum seeking algorithm is implemented online to find

online the optimal inductance and resistance respectively along constant-resistance and constant-inductance paths. The study has shown that the two paths are characterised by bell-shaped curves, which can be effectively "climbed" to the top by the extremum seeking algorithm. Indeed, on-line experiments have shown that the proposed local tuning of the five piezoelectric patches generates reductions of the resonant responses of the first, second and fourth flexural mode of the order of 14 dB, 4 dB, 8 dB.

## ACKNOWLEDGEMENTS

The support provided by the DEVISU project No 22017ZX9X4K006 funded by the PRIN 2017 programme of the Ministero dell'Istruzione, dell'Università e della Ricerca is acknowledged.

## REFERENCES

[1] J. Høgsberg and S. Krenk, "Balanced calibration of resonant shunt circuits for piezoelectric vibration control", J. Intell. Mater. Syst. Struct., vol. 23, no 17, p. 1937–1948, Nov 2012.
[2] P. Soltani, G. Kerschen, G. Tondreau, and A. Deraemaeker, "Piezoelectric vibration damping using resonant shunt circuits: an exact solution", Smart Mater. Struct., vol. 23, no 12, p. 125014, 2014.
[3] M. Berardengo, A. Cigada, S. Manzoni, and M. Vanali, "Vibration Control by Means of Piezoelectric Actuators Shunted with LR Impedances: Performance and Robustness Analysis", Shock Vib., vol. 2015, p. e704265, May 2015.
[4] P. Gardonio and D. Casagrande, "Shunted piezoelectric patch vibration absorber on two-dimensional thin structures: Tuning considerations", J. Sound Vib., vol. 395, p. 26–47, May 2017.
[5] O. Thomas, J. Ducarne, and J.-F. Deü, "Performance of piezoelectric shunts for vibration reduction", Smart Mater. Struct., vol. 21, no 1, p. 015008, 2011.
[6] P. Gardonio, E. Turco, "Tuning of vibration absorbers and Helmholtz resonators based on modal density/overlap parameters of distributed mechanical and acoustic systems", J Sound Vib, vol 451, 2019.
[7] J. J. Hollkamp and T. F. Starchville, "A Self-Tuning Piezoelectric Vibration Absorber", J. Intell. Mater. Syst. Struct., vol. 5, no 4, p. 559–566, Jul 1994.
[8] A. J. Fleming and S. O. R. Moheimani, "Adaptive piezoelectric shunt damping", Smart Mater. Struct., vol. 12, no 1, p. 36–48, Feb 2003.
[9] D. Niederberger, A. Fleming, S. O. R. Moheimani, and M. Morari, "Adaptive multi-mode resonant piezoelectric shunt damping", Smart Mater. Struct., vol. 13, no 5, p. 1025–1035, Oct 2004.
[10] P. Gardonio, E. Turco, A. Kras, L. D. Bo, and D. Casagrande, "Semi-active vibration control unit tuned to maximise electric power dissipation", J. Sound Vib., vol. 499, p. 116000, May 2021.
[11] P. Gardonio, M. Zientek, and L. Dal Bo, "Panel with self-tuning shunted piezoelectric patches for broadband flexural vibration control", Mech. Syst. Signal Process., vol. 134, p. 106299, Dec 2019.
[12] G. K. Rodrigues, P. Gardonio, L. Dal Bo, E. Turco, "Piezoelectric patch vibration control unit connected to a self-tuning RL-shunt set to maximise electric power absorption", J. Sound Vib., vol. 536, p. 117154, 2022.
[13] K. B. Ariyur and M. Krstic, Real-Time Optimization by Extremum-Seeking Control. John Wiley & Sons, 2003.
[14] L. Dal Bo, P. Gardonio, D. E. Casagrande, and S. Saggini, "Smart panel with sweeping and switching piezoelectric patch vibration absorbers: Experimental results", Mech. Syst. Signal Process., vol. 120, p. 308–325, Apr 2019.